Cutaneous immuno-surveillance and regulation of inflammation by group 2 innate lymphoid cells

Ben Roediger[1], Ryan Kyle[2], Kwok Ho Yip[3], Nital Sumaria[1], Thomas V. Guy[1], Brian S. Kim[4,5,6], Andrew J. Mitchell[1], Szun S. Tay[1], Rohit Jain[1], Elizabeth Forbes-Blom[2], Xi Chen[7], Philip L. Tong[1], Holly A. Bolton[1], David Artis[4,5,8], William E. Paul[7], Barbara Fazekas de St Groth[1,9], Michele A. Grimbaldeston[3], Graham Le Gros[2], and Wolfgang Weninger[1,9,10]

[1]The Centenary Institute, Newtown, NSW 2042, Australia [2]Malaghan Institute of Medical Research, Wellington, New Zealand [3]Centre for Cancer Biology, SA Pathology, Adelaide, South Australia, Australia [4]Department of Microbiology, Perelman School of Medicine Philadelphia, PA 19104, USA [5]Institute for Immunology, Perelman School of Medicine Philadelphia, PA 19104, USA [6]Department of Dermatology, Perelman School of Medicine Philadelphia, PA 19104, USA [7]National Institute of Allergic Disease, National Institutes of Health, Bethesda, Maryland, USA [8]Department of Pathobiology, School of Veterinary Medicine, University of Pennsylvania, Philadelphia, PA 19104, USA [9]Discipline of Dermatology, University of Sydney, Camperdown, NSW 2006, Australia [10]Department of Dermatology, Royal Prince Alfred Hospital, Camperdown, NSW 2050, Australia

Abstract

Type 2 immunity is critical for defense against cutaneous infections, but also underlies the development of allergic skin diseases. We report the identification in normal murine dermis of an abundant, phenotypically unique group 2 innate lymphoid cell (ILC2) subset that depends on interleukin 7 (IL-7) and constitutively produces IL-13. Intravital multiphoton microscopy revealed that dermal ILC2 specifically interact with mast cells, whose function was suppressed by IL-13. Treatment of $Rag1^{-/-}$ mice with IL-2 resulted in the expansion of activated, IL-5-producing dermal ILC2, leading to spontaneous dermatitis characterized by eosinophil infiltrate and activated mast cells. Our data show that ILC2 exhibit both pro- and anti-inflammatory properties and uncover a novel interactive pathway between two innate immune cell populations implicated in type 2 immunity and allergic diseases.

INTRODUCTION

The skin is the outermost barrier between the environment and internal organs that contains cells of the immune system deployed as sentinels and serving as a first line of defense against microbial attacks. The epidermis of mice harbors two relatively uniform populations of immune cells, Langerhans cells and dendritic epidermal T cells (DETCs), while the dermis contains a large variety of leukocytes, including dermal dendritic cells (DDCs), macrophages, mast cells and αβ and γδ T cells. It is believed that most of the productive immune responses against invading microbes are initiated in the dermis, although the precise lineage relationship of dermal leukocyte subsets and their exact functions during homeostasis and disease is yet to be defined.

Type 2 cytokine-dependent responses are essential for protection against helminth infections, but also underlie the development of inflammatory allergic diseases, such as atopic dermatitis[1]. Although over-production of epidermal-associated innate cytokines, for example thymic stromal lymphopoietin (TSLP)[2], has been associated with the development of cutaneous allergic sequelae, the cellular events in the skin which could be responsible for biasing subsequent immune responses to a T_H2 (atopic) phenotype have not been identified. In particular, there is no information as to whether an innate type 2 sensor is present in the dermis.

Recently, a novel class of innate lymphoid cells (ILC), group 2 ILC (ILC2; ref. 3), has been identified in fat-associated lymphoid tissue and mucosa-associated tissues (respiratory and intestinal tracts), on the basis of interleukin 25 (IL-25) responsiveness and the production of type 2 cytokines, the foremost being IL-13 (refs. 4–8). Cells that belong to the ILC2 family include natural helper (NH) cells[7], nuocytes[8] and innate helper 2 (Ih2) cells[9]. ILC2 are defined as lineage-negative (Lin⁻) CD45+CD90+CD127 (IL-7Rα)+ICOS+ with variable expression of CD117 (c-Kit), Sca-1 and ST2 (IL-33 receptor). Nuocytes have been shown to differentiate from common lymphocyte progenitors and to depend on the transcription factor RORα[10]. In adult mice, ILC2 are a rare cell population that expands in response to IL-25, IL-33 or during helminth infection[8] and represent a major source of IL-13, a pleiotropic cytokine that mediates a variety of effects including suppression of monocyte cytokine production[11], mucus production by goblet cells and eosinophil recruitment by epithelial cells[12–14]. ILC2 can also produce IL-5, implicated in eosinophil recruitment, and IL-9 (ref. 15) which is prominent during helminth infections[16, 17] and has been linked to atopic disease[18]. ILC2 have been shown to play a role in immunity against helminths as well as in allergic conditions such as asthma and chronic sinusitis[4, 5, 7, 8], but are also likely to be important for maintaining tissue homeostasis[6]. Despite recent advances, very little is understood about the behavior of ILC2 *in situ*, and it remains unclear what other cell types ILC2 interact with *in vivo*.

Here we describe the phenotype, developmental requirements and *in situ* behavior of a unique population of CD103+ ILC2 within the skin, which we have termed dermal ILC2 (dILC2). These cells depend on IL-7 for their survival and produce IL-13 during steady-state conditions. dILC2 continuously screen the dermis, where they preferentially interact with skin-resident mast cells. We further show that dILC2 respond to systemic treatment with

IL-2–anti-IL-2 complexes to proliferate and produce IL-5, which in turn promotes eosinophil influx and cutaneous inflammation. Taken together, dILC2 emerge as distinct dermal residents with the potential to initiate type 2 immune responses as well as exerting regulatory function on other dermal immune cell populations.

RESULTS

Identification of skin-resident CD103⁺ ILC2

We sought to determine whether murine skin might contain ILC2, defined, at least in part, by their absence of lineage markers and expression of CD90 (Thy-1) and the costimulatory molecule ICOS[8]. Using CD2 to exclude NK and NKT cells (Supplementary Fig. 1), we identified a population of CD45⁺CD11b⁻CD90^hiCD3⁻CD2⁻ ILCs in the skin of wild-type mice (Fig. 1a), which predominantly localized to the dermis at approximately one-third the abundance of T cells (Fig. 1b). These cells expressed ICOS (Fig. 1c), consistent with an ILC2 phenotype. The same staining strategy also identified an equivalent population in the mesentery (Fig. 1c), most likely corresponding to the natural helper cells previously described[7]. However, unlike the mucosal populations, skin ILC2 uniquely expressed CD103 (Fig. 1d), a molecule expressed by some skin-resident leukocytes, particularly T cells[19]. Further phenotypic analysis of this population revealed a lack of key T and NK cell markers together with expression of markers associated with ILC2, notably the high affinity IL-2 receptor (CD25), Sca-1 and ST2 (Supplementary Fig. 2). In contrast to ILC2 in other tissues, we were unable to detect expression of CD117 (c-Kit) by skin ILC2, but they did express the IL-25 receptor IL-17BR. We have therefore termed these cells dermal ILC2 (dILC2).

We also observed CD45⁺CD3⁻CD2⁻CD90^hi cells in other tissues, including blood and skin-draining lymph nodes (Fig. 1e and data not shown), but their relative abundance within the total leukocyte pool was very low for these tissues, particularly in comparison to the dermis, where dILC2 comprised 5–10% of all isolated CD45⁺ cells (Fig. 1f). We concluded that the dermis contains an abundant, phenotypically distinct population of ILC2.

Developmental requirements for dILC2 *in vivo*

We next determined the developmental requirements of dILC2 *in vivo*. Since many skin cells, including Langerhans cells, DETCs and dermal γδ T cells, are largely or partially radio-resistant[19], we first addressed the radio-sensitivity of dILC2. CD45.1⁺ recipient mice were sub-lethally irradiated and reconstituted with CD45.2⁺ bone marrow. Eight weeks post-irradiation, dILC2 were predominantly of donor origin, in contrast to radio-resistant CD3^hi DETCs (Fig. 2a). Since nuocytes have recently been shown to be derived from common lymphoid progenitors (CLPs)[10], we tested whether dILC2 were dependent upon the transcription factor Ikaros, which is essential for CLP generation and subsequent development of 'lymphoid' cells[20]. We made use of *Ikzf1*^L/L mice, in which the β-galactosidase reporter was inserted into the Ikaros locus[21]. *Ikzf1*^L/L mice are not completely deficient in Ikaros but are nevertheless incapable of achieving wildtype activity. To address dILC2 reliance upon Ikaros, wild-type (CD45.1⁺) mice were sub-lethally irradiated and reconstituted with 50:50 mG/mT (ubiquitous mTomato-expressing cells)[22]:wild-type (control) or 50:50 mG/mT:*Ikzf1*^L/L (test) bone marrow and examined 6–8 weeks later. The

percentage of donor-derived (CD45.2$^+$) mTomato$^-$ dILC2 was strongly reduced in test chimeras (Fig. 2b), indicating that dILC2 are highly dependent upon Ikaros for their development, consistent with a lymphoid origin for these cells.

To further explore their developmental and homeostatic requirements, we evaluated dILC2 in various genetically deficient mice. dILC2 were present in *Rag1*$^{-/-}$, NOD SCID and *Foxn1*$^{nu/nu}$ (nude) mice (Fig. 2c, Supplementary Fig. 3 and data not shown), confirming that they are not a T cell population and do not require the thymus for their development. dILC2 were absent from *Jak3*$^{-/-}$ mice[23] (Fig. 2c,d), indicating a requirement for signaling through the common gamma chain for their development or maintenance. While dILC2 numbers were unaffected in IL-15- and IL-2-deficient mice (Fig. 2c,d and data not shown), they were absent from IL-7-deficient skin (Fig. 2e). Collectively, these data indicate that dILC2 share the same developmental requirements as nuocytes[10] and natural helper cells[7]. Of note, dILC2 numbers were increased in *Rag1*$^{-/-}$ and other T cell-deficient mice (Fig. 2d, Supplementary Fig. 3) possibly due to an increase in IL-7 availability.

Given the apparent propensity of nuocytes to expand in response to IL-25 (ref. 8), we also tested whether dILC2 were present in *Il25*$^{-/-}$ mice. Lack of IL-25 had no effect on dILC2 numbers (Fig. 2f), indicating that IL-25 alone is dispensable for dILC2 homeostasis during the steady state.

Production of IL-13 by dILC2

Using reporter mice and intracellular cytokine staining, nuocytes and other innate helper cells have been reported to produce IL-13 (refs. 7–9) and small amounts of IL-4 (ref. 24). To test whether dILC2 might similarly produce IL-13 and IL-4, we utilized a dual reporter transgenic mouse, designated 4C13R (*Il4*-AmCyan *Il13*-dsRed), which expresses AmCyan under *Il4* regulatory elements and dsRed under *Il13* regulatory elements (Fig. 3a and **Methods**). 4C13R mice report cellular expression of *Il4* and *Il13* without affecting endogenous IL-4 and IL-13 production. 4C13R mice were healthy, viable and exhibited a robust IgE response to *Nippostrongylus brasiliensis* infection (Fig. 3b), while AmCyan and dsRed fluorescence was readily detectable in 4C13R T cells cultured under T$_H$2-inducing conditions (data not shown).

When we examined the skin of 4C13R mice, we found that dsRed-expressing cells were exclusively CD45$^+$CD90^{hi} and comprised mostly CD3$^-$NK1.1$^-$ dILC2 and some epidermal CD3^{hi} DETCs, the latter expressing lower *Il13*-dsRed compared to dILC2 (Fig. 3c and data not shown). *Il13*-dsRed expression by dILC2 was unaffected in *Il25*$^{-/-}$ mice (Fig. 3d). Furthermore, IL-13 protein was consistently detected in all wild-type skin samples examined but was significantly reduced in *Il7*$^{-/-}$ mice (Fig. 3e), indicating that dILC2 produce IL-13 during the steady-state.

In contrast to *Il13*-dsRed expression, dILC2 from 4C13R mice did not express AmCyan (Fig. 3f), indicating that these cells do not produce IL-4 during the steady-state. dILC2 in *Il4*$^{+/gfp}$ knockin mice[25] were similarly GFP-negative (Fig. 3g). Since it has recently been demonstrated that human ILC2 are capable of producing IL-4 in response to TSLP *in vitro*,[26] we tested whether dILC2 might similarly respond to TSLP *in vivo*. We examined

GFP expression by dILC2 in $Il4^{gfp/gfp}$ mice following topical application with the vitamin D analogue, MC903, which has previously been shown to induce TSLP expression by skin keratinocytes[27]. MC903 induced substantial production of TSLP in treated ears compared to vehicle treated controls (Fig. 3h). Following exposure to MC903, a small but reproducible population of dILC2 expressed $Il4$-eGFP in TSLP receptor-sufficient but not TSLPR-deficient mice (Fig. 3i). IL-4 protein was not detectable in MC903-treated skin (data not shown), while IL-13 production by dILC2 appeared modestly increased, though this did not reach statistical significance (Supplementary Fig. 4). We concluded that dILC2 produce IL-13 but not IL-4 during the steady-state, but that IL-4 may be generated under defined inflammatory conditions.

Visualization of dILC2 *in vivo*

To visualize dILC2 *in situ*, we made use of mice with an eGFP knock-in at the *Bonzo*/*Cxcr6* locus[28] ($Cxcr6^{+/gfp}$ mice). In these mice, a number of lymphoid populations express eGFP, including some T cell subsets and RORγt[+] ILCs[29]. Flow cytometric analysis of Lin[−]Sca-1^{+} natural helper cells[7] in the mesentery of $Cxcr6^{+/gfp}$ demonstrated bright fluorescence in approximately 50% of these cells (Fig. 4a). In the skin, almost all dILC2 expressed eGFP (Fig. 4b). The ease with which eGFP^{+} cells can be imaged in the skin of $Cxcr6^{+/gfp}$ mice[19] enabled us to determine the density of dILC2 in the mouse skin to be 50–100 cells/mm^{2} (Fig. 4c; see **Methods** for details).

To visualize dILC2 exclusively, we exploited their radiosensitivity and generated mixed bone marrow chimeras in which bone marrow from $Rag1^{−/−}$ $Cxcr6^{+/gfp}$ mice was co-injected with RAG-1-sufficient, GFP[−] mTomato[+] mG/mT bone marrow into irradiated recipients. Flow cytometric analysis confirmed that eGFP expression in the skin of recipient mice was confined to CD90^{hi}CD3^{−}CD2^{−} dILC2, with only a minor contribution of CD3^{−}CD2^{+} NK cells (Fig. 4d). eGFP^{+} dILC2 were readily detectable by multiphoton microscopy (Fig. 4e), where they exhibited a distinct migratory phenotype (Supplementary Video 1). In contrast to cutaneous T cells, the average speed of dILC2 rarely exceeded 5 μm/min, and was characterized by brief migratory periods followed by extended pauses (Fig. 4f and Supplementary Video 2). Thus, while dILC2 instantaneous speed could exceed 10 μm/min (Fig. 4g), their average speed was similar to that of migratory DDCs[30]. The total displacement of dILC2 within a 15-minute time frame was also attenuated compared to the faster-moving T cells (Fig. 4h), whereas the mean meandering indices were almost identical (Fig. 4i). Despite the lower migratory speed, these data nevertheless demonstrated that dILC2 patrol their local environment, consistent with a potential immuno-surveillance function.

The presence of donor-derived mTomato-expressing cells in these mixed chimeras enabled us to address whether dILC2 interacted with radiosensitive leukocytes in the skin, particularly dermal macrophages and DCs (Fig. 4e). Despite the high prevalence of mTomato[+] mG/mT-derived antigen presenting cells (APCs) in the ears of mixed chimeric mice, dILC2 interactions with these cells were infrequent and transient (Supplementary Videos 3,4). Similarly, when triple-chimeric mice were generated, in which bone marrow from CD11c-eYFP mice was included to visualize DDCs, sustained dILC2 interactions with

eYFP[+] DDCs and mTomato[+] APCs were not observed (Supplementary Video 5 and data not shown).

Although we did not see many dILC2 interactions with APCs, the frequent stationary behavior of dILC2 nevertheless suggested that these cells did form stable contacts with another, presumably radio-resistant cell population. While this population could include non-hematopoietic cells such as endothelial cells and fibroblasts, we were particularly interested in whether dILC2 were interacting with mast cells, given their role as an effector population in type 2 immune responses[31] and their resistance to irradiation (data not shown). To explore this possibility, we exploited our observation that Brainbow transgenic mice[32] can be used as mast cell reporter mice. We had found that, in addition to red fluorescent protein (RFP, mTomato) expression in central and peripheral neurons in Brainbow mice, RFP is also expressed by some skin leukocytes (Fig. 5a), including a population of RFP[dim]MHC-II[hi] migratory DDCs and a non-migratory population of predominantly perivascular RFP^{hi}MHC-II^{lo} cells (Fig. 5b, Supplementary Video 6). Phenotypic analysis by flow cytometry demonstrated that these RFP^{hi} cells were CD11b^{lo}Fc"R1^{+}c-Kit^{+} mast cells (data not shown), which was confirmed by the co-expression of RFP and eGFP in the progeny of Brainbow mice crossed to c-Kit-eGFP mast cell reporter mice[33] (Fig. 5c).

To test whether dILC2 interacted with mast cells *in vivo*, we generated Brainbow × *Cxcr6*[+/gfp] mice and assessed the skin by multiphoton microscopy. eGFP^{+} cells could be observed in close proximity to RFP^{hi} mast cells within these mice (Fig. 5d). These apparent interactions often lasted the entire recording session of 10–30 minutes (Supplementary Video 7). To visualize dILC2 exclusively, without the presence of eGFP^{+} T cells, we generated mixed bone marrow chimeras in which bone marrow from *Rag1*^{−/−} *Cxcr6*[+/gfp] mice was co-injected with RAG-1-sufficient, GFP[−] bone marrow into irradiated Brainbow mice. As before, eGFP expression was largely restricted to dILC2 (Fig. 5e), while RFP expression was restricted to radioresistant mast cells. Intravital multiphoton imaging of these mice demonstrated that not only did dILC2 migrate in close proximity to skin-resident mast cells (Fig. 5f, Supplementary Video 8,9), but that dILC2 also formed stable interactions with mast cells that lasted over 20–30 minutes (Fig. 5g, Supplementary Video 10).

Despite these sustained interactions, mast cells did not appear to be important for dILC2 occupation and/or survival in the skin, as both the frequency and absolute numbers of dILC2 in the skin of mast-cell deficient B6-*Kit*[W-sh/W-sh] and WBB6F_1-*Kit*[W/W-v] mice[34] did not differ from their respective controls (Fig. 5h,i).

To examine how interactions between dILC2 might affect mast cell biology, in particular the role of ILC2-produced cytokines such as IL-13 and IL-9, we utilized a well-established *in vitro* model in which IgE-dependent release of IL-6 and tumor necrosis factor (TNF) by pre-sensitized bone-marrow-derived mast cells was measured in the presence or absence of recombinant IL-13 or IL-9 (ref. 35). Co-incubation with IL-13 had a dose-dependent suppressive effect on IgE-dependent cytokine release by mast cells (Fig. 5j,k). This suppression was specific, as co-incubation with IL-9 conversely enhanced IL-6 and TNF production under the same protocol (Supplementary Fig. 5). These data suggest that dILC2 have the potential to modulate mast cell function through the production of IL-13.

IL-2 induced activation and proliferation of ILC2 *in vivo*

We sought to address the function of dILC2 *in vivo*. Although antibody depletion approaches have been used successfully to evaluate the role of lung ILC2 *in vivo*,[4, 36] dILC2 appear to be resistant to such strategies, since both anti-CD90.2 and anti-CD25 failed to deplete dILC2 from *Rag1*^{−/−} mice, even when splenic ILC2 were effectively cleared (Supplementary Fig. 6). We therefore sought to activate dILC2 directly *in vivo* to stimulate cytokine production. In contrast to NK cells and NKp46^{+} ILCs, ILC2 were unique in their expression of the high affinity IL-2 receptor (Supplementary Fig. 7), and were the predominant CD25-expressing hematopoietic population in *Rag1*^{−/−} mice. Since ILC2 have been shown to respond to IL-2 *in vitro* by producing IL-5, IL-9 and IL-13 (refs. 4, 15, 36), we tested if IL-2 might also activate these cells *in vivo* by injecting *Rag1*^{−/−} mice with IL-2–JES6-1 antibody complexes every second day for 1–3 weeks. Co-administration of IL-2 with clone JES6-1, an IL-2-specific monoclonal antibody, has previously been shown to selectively expand CD25-expressing regulatory T cells in wild-type mice without activating cells such as NK cells that express the low affinity IL-2 receptor[37]. After two weeks of treatment, splenic ILC2 populations were expanded approximately 5-fold in *Rag1*^{−/−} mice (Fig. 6a), indicating that IL-2 stimulated proliferation of these cells. As expected, NK cells were unaffected (Fig. 6b and data not shown). IL-2-expanded ILC2 displayed an activated phenotype, characterized by increased surface expression of CD25, ICOS, CD69 and T1/ST2, while some adhesion molecules, namely integrin β_7 and CD49d, were down regulated (Fig. 6c and Table 1).

In the skin, dILC2 population expansion in response to IL-2–JES6-1 was even more marked, with an approximately 10-fold increase in absolute numbers after 2 weeks of treatment (Fig. 7a). To visualize these cells, we treated *Rag1*^{−/−} *Cxcr6*[+/gfp] mice with IL-2–JES6-1 for two weeks and then assessed the skin by multiphoton microscopy. *Cxcr6*-eGFP[+] dILC2 were markedly increased and predominantly located in close proximity to blood vessels (Fig. 7b). Intravital imaging of these mice revealed that activated dILC2 exhibited the same heterogeneous migratory phenotype as was observed during the steady-state, such that some dILC2 migrated but a large proportion remained stationary throughout the imaging period (Supplementary Video 11).

Of note, we routinely observed vascular leakage of Evans blue when imaging IL-2-treated mice, indicative of inflammation (Supplementary Fig. 8a). We therefore assessed the cytokine profile of skin from IL-2-treated mice, which revealed increased IL-5 and IL-13 protein production, consistent with the dILC2 expansion and activation (Fig. 7c), but also increased inflammatory cytokines such as IL-6, TNF and CXCL1 (Fig. 7d). IL-3, IL-4, IL-9, IL-17 and interferon-γ were not detected in either IL-2-treated or control mice, while TSLP and IL-25 concentrations were unchanged between the two groups (data not shown). Consistent with the increased IL-5 and CXCL1, IL-2-treated skin contained dermal leukocyte infiltrates consisting of eosinophils and neutrophils (Supplementary Fig. 8b and data not shown). To test whether the increased IL-5 and IL-13 was due to increased production of these cytokines by dILC2, we sorted CD45^{+}CD90^{hi}CD2^{−} dILC2 from untreated and IL-2-treated *Rag1*^{−/−} mice and examined *Il5* and *Il13* mRNA abundance by RT-qPCR. dILC2 expression of both *Il13* and *Il5* was markedly increased following

treatment with IL-2–JES6-1, indicating that IL-2-expanded dILC2 are functionally distinct from steady-state dILC2 (Fig. 7e), whereas as expression of *Gata3* (refs. 26, 38) remained unchanged.

We observed that over 50% of *Rag1*^{−/−} mice spontaneously developed clinically overt inflammatory skin lesions within 2–3 weeks of IL-2–JES6-1 treatment, particularly on or around the ears, eyes, mouth and tail (Fig. 7f and data not shown). Histologically, these lesions exhibited epidermal hyperplasia, dermal thickening and extensive eosinophil and neutrophil influx throughout the dermis and epidermis (Fig. 7g,h, Supplementary Fig. 8c). Additionally, skin mast cells displayed a degranulated morphology in IL-2-treated skin (Fig. 7i), particularly in regions with leukocyte infiltration (Supplementary Fig. 8d). We concluded that IL-2-activated dILC2 promote cutaneous inflammation, mediated at least in part by increased IL-5 production and eosinophil recruitment.

DISCUSSION

The skin is important for the early recognition of infection- and environmentally-derived antigens and for the development of the appropriate Th1, Th2, or Th17 subset bias, both of which are critical for resolution of the challenge. Given the importance of the many allergic and parasitic diseases linked to type 2 immunity, a better understanding of the regulatory cues involved in their generation is imperative. In contrast to the well-established type 1 initiating cells in the dermis, such as IL-12-producing migratory DDC and IL-17 producing γδ T cells,[19] the existence of an equivalent dermal leukocyte subset driving downstream Th2 immunity remains speculative. Type 2 cytokine-producing ILC2 cells in the lung and gut have recently emerged as early responders following systemic parasitic infections and have also been implicated in the pathogenesis of allergic diseases such as asthma.[4, 24] In the current study, we have identified a novel population of skin-resident CD103^{+} dermal ILC2. In contrast to dILC2 in mucosa-associated tissues, those in the skin are already abundant in the steady-state and constitutively produce IL-13, but following activation they may expand and switch to a pro-inflammatory phenotype, characterized by markedly increased production of IL-5. dILC2 are responsive to TSLP and are able to express *Il4*, further underlining their likely importance as a type 2 sensor in the skin.

The near-exclusive production of IL-13 in the skin by dILC2 may have relevance for atopic skin conditions, given the evidence that IL-13 plays a major role in allergic inflammation, including atopic dermatitis.[39] Although the steady-state production of IL-13 by dILC2 implies a homeostatic function for this cytokine, it is nevertheless conceivable that dILC2-derived IL-13 also plays a role in atopic disease under more pathological conditions, particularly when the cytokine has better access to other cell populations such as endothelial cells and keratinocytes.[40]

It currently remains unclear whether dILC2 are a subset of circulating ILC2,[9] or whether they are a permanent skin-resident population. In the former case, ILC2 would appear to be highly skin-trophic, given their high relative abundance in the dermis compared with blood and other organs. Indeed, we estimate that there are more dILC2 residing in two mouse ears than can be found within the entire spleen. Thus, ILC2 are not as rare as previously believed,

but do have a greater propensity for non-lymphoid tissues, particularly the skin. The increased prevalence of dILC2 in $Rag1^{-/-}$ mice and severely diminished numbers in $Il7^{-/-}$ mice suggests that ILC2 compete with T cells for IL-7, analogous to the increased prevalence of NK cells in $Rag1^{-/-}$ mice due to improved IL-15 bioavailability.[41]

An important aspect of leukocyte function is their migratory and interactive behavior within intact tissues. Our *in vivo* imaging experiments have revealed that, despite their developmental and phenotypic similarities, dILC2 differed markedly from T cells in their behavior within the skin. dILC2 characteristically migrated in bursts followed by extensive pauses. These periods of migratory arrest appeared result from encounters with skin-resident mast cells. The physical proximity of these two cell types supports the notion that ILC2 can directly influence mast cell function and *vice versa*, and that such influence need not be restricted to secreted cytokines, but could result from receptor-ligand interactions. Thus, intravital imaging has revealed an unexpected partnership between two type 2 immune cells *in vivo* that is likely to be important in both steady-state and inflammatory conditions.

Finally, we demonstrate that ILC2 can be directly activated and expanded *in vivo* using IL-2–anti-IL-2 complexes, which has enabled us to directly compare the phenotype of steady-state ILC2 to activated ILC2 *in vivo* and to assess the impact of dILC2 stimulation on cutaneous inflammation. We found that *in vivo*-stimulated ILC2 exhibit a distinct phenotypic signature, characterized by increased levels of surface CD25, ICOS and ST2. In the skin, activated dILC2 markedly increased IL-5 production, which resulted in eosinophil recruitment and predisposed the mice to spontaneous dermatitis. The occurrence of spontaneous lesions at sites that are routinely exposed to body fluids (tears and/or saliva) or minor traumas (ears, tail) is consistent with the existence of an external trigger, which presumably initiates a cascade of immunological events following keratinocyte activation.

The relevance of the ILC2 responsiveness to IL-2 in immuno-competent mice requires future investigation. It is likely that ILC2 function *in vivo* is regulated, at least in part, by T cells, since the predominant source of IL-2 in wild-type mice is activated T cells, and the bioavailability of IL-2 is in turn influenced by the number of regulatory T cells.[42] By extension, ILC2 could represent an important downstream effector mechanism within the adaptive immune response. Indeed, evidence for T cell-dependence of ILC2 expansion during helminth infection has already been reported,[8] although IL-2 was not suggested as the underlying mechanism. Regardless, our data demonstrate that activation of dILC2 by IL-2 alone is sufficient to promote cutaneous inflammation, and that these cells can represent a potent effector population under the appropriate conditions.

The distinct phenotypic and functional differences between untreated and IL-2-treated dILC2 demonstrate that these cells can exhibit at least two functionally distinct states *in vivo*. During the steady-state, dILC2 likely take on an immunoregulatory role, in which dILC2-produced IL-13 serves to moderate mast cell activity. In contrast, once stimulated, dILC2 become pro-inflammatory, capable of promoting eosinophil influx and mast cell activation. Taken together, these data demonstrate that dILC2 represent an abundant, phenotypically unique population of group 2 innate lymphoid cells in the skin that plays an important role in the regulation of cutaneous inflammation. These findings may be of

relevance to a number of inflammatory skin conditions in which eosinophil recruitment is a defining feature, including atopic skin disease and parasite infections.

METHODS

Mice

Transgenic mice expressing AmCyan under *Il4* regulatory elements and destabilized dsRed (dsRed-DR) under *Il13* regulatory elements (4C13R mice) were prepared using BAC-recombineering technology with *galK*-selection. A BAC-clone (RP23.97H11) containing the T_H2 locus control region (LCR) and the *Il13,* CNS-1, *Il4*, VA and *Kif3a* genes or regions was obtained from the Children's Hospital of Oakland Research Institute. The color plasmids p-AmCyan1-N1 and p-dsRed-Express-DR were from Clontech. The starting ATG codon of the *Il4* gene in BAC RP23.97H11 was targeted with a *galK* cassette containing 5′ and 3′ homology arms from the *Il4* gene. In the resultant "*Il4 galK*" BAC, the *galK* was then targeted with an AmCyan construct, which replaced *galK*, thus placed the AmCyan into the correct site within the *Il4* gene of the BAC. Use the same principle, the *galK* cassette was targeted with the starting ATG codon of the *Il13* gene of "*Il4*-AmCyan" BAC, containing 5′ and 3′ homology arms from the *Il13* gene. In the resultant "*Il13 galK*–*Il4*-AmCyan" BAC, the *galK* was targeted with a dsRed-DR construct which replaced the *galK*. This placement was verified by fully sequencing the region between 5′ and 3′ homology regions on the *Il13*-dsRed-DR–*Il4*-AmCyan BAC. The BAC was linearized by digestion with Asc1 and the lineage fragment containing T_H2 *Lcr*, *Il13*-dsRed-DR*,* CNS-1, *Il4*-AmCyan, VA and *Kif3a* was size verified by PCR. The fragment was then microinjected into C57BL/6 oocytes. These oocytes were subsequently transferred into pseudo-pregnant foster mothers of C57BL/6 background. To identify which offspring expressed the construct, Southern blot analysis was performed. The genomic DNA of potentially transgenic pups was isolated. DNA was digested with BamHI, separated on 0.8% agarose gel, transferred to nylon membrane and probed with a 916 bp PCR fragment spanning the 5′ and 3′ homology arms of the *Il13*-dsRed-DR construct. As a positive control, the purified BamHI-digested *Il13*-dsRed-Express-DR–BAC RP23.97H11 construct that was used for initial microinjections was run in parallel with the genomic DNA samples.

All mice used were on a C57BL/6 background, unless otherwise specified. BALB/c, C57BL/6, B6.SJL/Ptprc[a] (CD45.1), *Rag1*^{−/−}, NOD SCID (NOD.CB17-Prkdc[scid]/ARC) and *Foxn1*[nu/nu] (nude) mice were purchased from the Animal Research Centre (Perth, Australia). *Tcrb*^{−/−} and *Tcrd*^{−/−} mice, mG/mT mice[22], *Cxcr6*[+/gfp] mice[28], *Il2*^{−/−} mice and Brainbow (B6;CBA-Tg(Thy1-Brainbow1.0)LLich/J) mice[32] were purchased from The Jackson Laboratory. *Rag2*^{−/−} and mice were purchased from Taconic. c-Kit-eGFP mice[33] were provided by P. Besmer (Sloan Kettering Institute). *Ikzf1*[L/L] mice have been described previously.[43] *Il7*^{−/−} mice[44], *Il15*^{−/−} mice[45] and *Jak3*^{−/−} mice[23] were provided by J.H. Cho and J. Sprent (Garvan Institute, Sydney, Australia). *Il25*^{−/−} mice[46] were provided by M. Kleinschek (DNAX). *Il3*^{−/−} mice (BALB/c) have been described previously.[47] *Il4*[gfp/gfp], *Il4*[+/gfp] mice (BALB/c) and *Tslpr*^{−/−} mice[48] were obtained from the National Institutes of Health. B6-*Kit*[W-sh/W-sh] and WBB6F[1]-*Kit*[W/W-v] mice[34] were bred and maintained at the Institute of Veterinary and Medical Science animal facility, Adelaide[34, 35]. CD11c-eYFP

mice have been described previously[30]. C57BL/6-C[2J] (albino B6) mice have been described previously.[49] $Il25^{-/-}$ 4C13R and $Il4^{gfp/gfp}$ $Tslpr^{-/-}$ mice[48] were bred and maintained by the Malaghan Institute of Medical Research animal facility in Wellington, New Zealand. C57BL/6-C[2J] Brainbow (albino Brainbow) mice, Brainbow × c-Kit-eGFP mice, Brainbow × $Cxcr6^{+/gfp}$ mice and $Rag1^{-/-}$ $Cxcr6^{+/gfp}$ mice were generated at the Centenary Institute animal facility. All animal experiments were performed with the approval of the Animal Ethics Committee at the University of Sydney (Sydney, Australia), the Victoria University Animal Ethics Committee (Wellington, New Zealand) or the Institute of Medical and Veterinary Science Animal Ethics Committee (Adelaide, Australia).

Tissue processing and flow cytometry

Spleens, Peyer's patches and skin-draining (inguinal, axillary, brachial) and mucosal (mesenteric) lymph nodes were subjected to digestion with collagenase IV (0.5 mg/ml, Sigma) at 20–22°C for 30 min prior to filtration through an 80 μm stainless steel mesh to obtain single cell suspensions. Spleen cells were washed in running buffer (PBS, 5% FCS, 5 mM EDTA), followed by red blood cell lysis prior to cell counting and antibody staining. Spleen and lymph node samples were counted using a Sysmex XS-1000i Automated Hematology Analyzer (Toa Medical Electronics). Mesentery, as previously defined,[7] was carefully dissected and subjected to enzymatic digestion with collagenase IV (0.5mg/ml, Sigma) at 20–22°C for 30 min prior to filtration through an 80 μm stainless steel mesh to obtain single cell suspensions. Isolation of skin cells involved one of two processes: For whole skin preparations, ears were split into dorsal and ventral halves using forceps and subjected to enzymatic digestion with 2–5 mg/ml collagenase type IV in PBS (Sigma-Aldrich) for 60 min at 37°C to release cells. Alternatively, for dermal preparations, ears were split into dorsal and ventral halves using forceps and first subjected to enzymatic digestion with 5 U/ml dispase I in PBS (BD Biosciences) for 90 min at 37°C to allow for epidermal and dermal separation. Following epidermal separation, dermal halves were then digested in 2–5 mg/ml collagenase type IV in PBS for 45 min at 37°C. Tissues were filtered through an 80 μm stainless steel mesh to obtain single cell suspensions. For some digestions, skin leukocytes were released in 0.5 mg/mL Liberase TL ResearchGrade (Roche) in PBS for 60 min at 37°C and processed as above. Cells were washed in running buffer (PBS, 5% FCS, 20 mM EDTA) and counted volumetrically using AccuCount beads (Spherotech). To isolate lamina propria cells, small intestines were excised from mice after ventricle perfusion with Hank's Balanced Salt Solution (HBSS, Life Technologies). The mesentery and Peyer's patches were removed and intestinal contents flushed thoroughly with 25 ml HBSS + 5% FCS. 2 cm segments were sliced longitudinally and rinsed in serum-free HBSS. To remove epithelial sheets, flushed intestinal sections were agitated for 1min in HBSS containing 1mM EDTA by hand, followed by rocking for 15 min at 20–22°C (100 rpm, approx. 1.12g, Ratek Orbital Shaker Model OM11). Epithelial sheet removal was repeated before the tissue was diced and subject to collagenase digestion (1mg/ml Collagenase IV, Sigma, in HBSS + 5%FCS) for 30 min at 37°C (150 rpm, approx. 1.68g Ratek Orbital Shaker). Digested contents were triturated and filtered through 40 μm cell strainers. Cells were washed twice and pelleted at 500g before staining. Single cell suspensions were incubated with anti-CD16/32 (2.4G2; BD Biosciences) to block non-specific binding and stained with fluorochrome-conjugated antibodies made up in flow cytometry buffer (PBS containing 5%

FCS, 2 mM EDTA and 0.02% sodium azide). Fluorochrome-conjugated antibodies against the following cell surface molecules were used: CD2 (RM2-5), CD3 (145-2C11), CD4 (RM4-5), CD8 (53-6.7), CD11b (M1/70), CD25 (PC61), CD38 (90/CD38), CD43 (S7), CD44 (IM7), CD45 (30-F11), CD45R (RA3-6B2), CD45.2 (104), CD49b (DX5), CD49d (9C10(MFR4.B)), CD69 (H1.2F3), CD117 (2B8), CD132 (TUGm2), integrin β_7 (M293), MHC-II (2GB), NK1.1 (PK136), T1/ST2 (DJ8) (BD Biosciences), CD5 (53-7.3), CD27 (LG.7F9), CD39 (24DMS1), CD90.2 (53-2.1), CD103 (2E7), CD122 (TM-b1), CD244.2 (eBio244F4), ICOS (7E.17G9), IL-13Ra1 (13MOKA), IL-15Ra (DNT15Ra), KLRG1 (2F1), NKG2D (CX5), NKp46 (29A7.4), Fc"R1 (MAR-1), Sca-1 (D7) (eBioscience), CD84 (MCD84.7), IL-13Ra1 (5H10-27(MFR5)) (BioLegend). Rabbit polyclonal anti-IL-17RB was purchased from Millipore. IgE-specific antibodies (clone 6HD5 and clone R1E4) were purified in house from hybridoma cell lines at the Malaghan Institute. DNP-specific antibodies (clone SPE-7) purified in house from the hybridoma cell line at Centre for Cancer Biology. For flow cytometry experiments, cell suspensions were re-suspended in running buffer containing 0.5 μg/ml 4′,6-diamidino-2- phenylindole dihydrochloride (DAPI) (Molecular Probes, Invitrogen) for dead cell exclusion. For phenotypic analysis experiments, the presence of other leukocytes bearing the marker of interest was a requisite internal positive control before concluding a lack of expression by dILC2, to exclude possible misinterpretation due to enzyme cleavage artifacts. Level of expression was compared against fluorescence-minus-one controls. Cells were analyzed on a FACS Canto (BD), an Accuri C6 (BD) or a 4- 5- or custom 10-laser LSR II cytometer (BD). Flow data were analyzed using Flowjo (Tree Star).

Generation of bone marrow chimeras

To create bone marrow chimeras, B6.SJL/Ptprc[a] (CD45.1) hosts were irradiated with 750 cGy (Gammacell 40 Exactor, Nordion International Inc., dual source [137]Caesium) irradiation. 24 h later, the irradiated hosts received $8–10 \times 10^6$ bone marrow cells from C57BL/6 (CD45.2) donor mice. For competitive repopulation experiments, B6.SJL/Ptprc[a] (CD45.1) hosts were sub-lethally irradiated with 750 cGy and received a bone marrow graft ($8–10 \times 10^6$ cells) consisting of mG/mT bone marrow mixed 1:1 with either wild-type C57BL/6 (CD45.2) bone marrow (control chimeras) or *Ikzf1*[L/L] bone marrow (for mixed chimeras) 24 h later. C57BL/6-C[2J] (albino B6) mice or C57BL/6-C[2J] Brainbow (albino Brainbow) mice were irradiated with 750 cGy and received a bone marrow graft ($8–10 \times 10^6$ cells) from indicated donor mice. All chimeric mice were allowed to reconstitute for at least 6 weeks before use in experiments.

Cytokine measurement of tissues

Cytokine content of tissue homogenate was measured using Cytometric Bead Array (CBA) assay (BD) or ELISA (TSLP, IL-25 and IL-33 Duoset, R&D Systems), with minor modifications from the manufacturer's protocol. Briefly, tissues were mechanically homogenized using a rotor stator homogenizer (Polytron) in PBS containing protease inhibitors (HaltTM protease inhibitor; Thermo Scientific) and 5 mM EDTA. The homogenate was then centrifuged 15,000*g* for 10 min at 4 °C. The resulting supernatant was then used for cytokine quantification, with all sample and reaction volumes scaled down to either 10% (CBA) or 25% (enhanced sensitivity CBA) of recommended volumes.

Cytokine levels were interpolated from standard curves generating using recombinant proteins (BD or R&D Systems). The amount of cytokine per gram of tissue was calculated to be = ([Volume of homogenate (ml) + tissue volume (ml)] × cytokine concentrations (pg/ml))/(tissue weight (g)), assuming a tissue density of 1mg/ml and 100% efficiency cytokine release into the homogenate.

IgE following infection with *Nippostrongylus brasiliensis*

Wild-type and 4C13R mice were infected with 600 live *Nippostrongylus brasiliensis* third-stage larvae via subcutaneous injection. Blood was collected via lateral vein bleeds on days 6, 9, 12, 15 post infection and spun at 1800g for 4 min and serum was collected and stored at -20 °C. Serum IgE was measured by ELISA. Plates were coated overnight at 4 °C with 100 μl anti-IgE (clone 6HD5) at 5μg/ml. Wells were blocked for 2 h with 10% FCS in PBS. Samples were diluted in 10% FCS in PBS and this was used as a blank, while a cell line-derived (12-3) IgE standard was used as a positive control. Samples and standards were then incubated at 20–22°C for 2 h before extensive washing and incubation in 100 μl biotinylated anti-IgE (clone R1E4, 3 μg/ml) for 2 h at 20–22°C. Samples were then incubated in 100 μl HRP Streptavidin (GE Healthcare Life Sciences) (1:1000) for 1 h at 20–22°C and plates developed with 100 μl BD OptEIA TMB Substrate (BD). Development was stopped with addition of 0.25M H_2SO_4.

Multiphoton intravital imaging of skin and image analysis

Preparation of animals and imaging was performed as previously described[19, 30]. In brief, mice were anesthetized by intraperitoneal injection of Ketamine/Xylazine (80/10 mg/kg), with repeated half-dose injections as required. The ears were treated with Nair® depilatory cream (Church and Dwight) to remove hairs. The animals were then placed onto a custom-built stage to position the ear on a small metal platform for multiphoton (MP) imaging. The ear was immersed in PBS/glycerin (70:30, vol:vol) and covered with a coverslip. Body temperature was kept at 37 °C using a heating pad placed underneath the mouse while the temperature of the platform was maintained independently at 35°C. In some experiments, mice were injected with Evans Blue for the detection of blood vessels. Multiphoton intravital imaging was performed using a LaVision BioTec TriMScope attached to an Olympus BX-51 fixed stage microscope equipped with a diode pumped, wideband mode-locked Ti:Sapphire femtosecond laser (MaiTai, SpectraPhysics) and an APE Optical Parametric Oscillator (OPO). Samples were imaged through a 20x or 16x water immersion objective. For fluorophore detection, samples were simultaneously exposed to polarized laser light at wavelengths of 920 nm for the excitation of GFP, YFP, Evans Blue and second harmonic generation and 1080 nm light from the OPO for excitation of mTomato or phycoerythrin. Three-dimensional (x, y, z) images of the ear skin were acquired (2–4 μm spacing in z-axis over indicated depth) every 30–60 s for a period of 0.5–2 h. Chromatic aberration between Ti:Sapphire and OPO-excited fluorophores was determined prior to imaging experiments using autofluorescent beads and adjusted for post-acquisition in ImageJ. In experiments involving CD11c-eYFP, GFP and YFP channels were spectrally unmixed post-acquisition using ImageJ. Migration parameters were determined using Volocity (PerkinElmer) as described previously[19, 30]. Image stacks were transformed into movies using ImageJ.

Enumeration of dILC2 density *in vivo*

Image stacks from *Cxcr6*[+/gfp] mice were acquired by multiphoton microscopy as described above. Images were collected every 2 μm in the *z*-axis throughout the entire depth of the ear (approx. 150 μm from the top of the epidermis). Mice were then sacrificed, and the ears digested using dispase as described above. Following separation of the epidermis from dermis and collagenase digestion, dermal samples were stained with antibodies against CD45, CD3, CD2, CD90 and CD11b and T, NK and dILC2 were then assessed for GFP fluorescence by flow cytometry. Quality of epidermal removal was assessed by the degree of CD3^{hi} DETC contamination and samples were considered sufficiently pure if DETC constituted less than 1% of total CD45^{+} cells. Multiphoton image stacks were processed using ImageJ software. Dermal GFP^{+} cells were identified by presence of SHG signal[30] and enumerated manually using the 'point' and 'multi-point' selection tools to determine the density of GFP^{+} cells within the skin. Using the flow cytometric data, the density of individual cell subsets was determined using the formula: density of cell type Y = [density GFP^{+} cells] × [percentage of GFP^{+} cells that are cell type Y]/[percentage of cell type Y that are GFP[+]].

Mast cell stimulation and cytokine measurement

As previously described[35], bone marrow-derived cultured mast cells (BMCMC) were obtained by culture of bone marrow progenitor cells from femurs and tibias of female mice for 4–6 weeks in 20% WEHI-3-conditional medium (containing IL-3); Purity of mast cell populations (> 95%) were identified by May-Grunwald-Giemsa staining and by flow cytometry (FcεR1[+]c-Kit[+]). BMCMC were incubated with IL-13 or IL-9 (Shenandoah Biotechnology Inc.) (0–10,000 pg/ml) and sensitized with IgE anti-DNP mAb (clone SPE-7) at 2 μg/ml in WEHI-3-conditioned medium overnight at 37 °C. BMCMCs were centrifuged for 5 min at 200*g*, resuspended at a density of 10^6 cells per ml in DMEM containing 1% (vol/vol) BSA (Sigma), and then stimulated with 20 ng/ml of DNP-HSA–specific antigen (Sigma) in the presence of IL-13 or IL-9 for 6 h. IL-6 and TNF in the supernatants were measured by enzyme-linked immunosorbent assay in accordance with the manufacturer's instructions (BD Bioscience).

ILC2 depletion by monoclonal antibodies *in vivo*

For depletion studies, *Rag1*^{−/−} mice were injected with either anti-CD25 (clone PC61) or anti-CD90.2 (clone 30H12) intraperitoneally with 200 μg antibody per day for two days prior to sacrifice and organ harvest. PC61 and 30H12 were grown and purified in house at the Malaghan Institute of Medical Research, Wellington, New Zealand.

In vivo treatment with IL-2/anti-IL-2

To expand ILC2, *Rag1*^{−/−} mice were treated with IL-2–JES6-1 antibody complexes as previously described[37]. Each injection consisted of 1 μg IL-2 (PeproTech) complexed to 5 μg JES6-1 antibody (WEHI monoclonal antibody Facility, Melbourne, VIC, Australia), which corresponded, approximately, to a 2:1 molar ratio of cytokine to antibody. IL-2–JES6-1 complexes were prepared by mixing IL-2 and JES6-1 antibody at the appropriate ratio and incubating for 30 min at 37°C. Aliquots were then frozen at −70°C until use.

Aliquots were resuspended in PBS immediately before use and injected intraperitoneally in a volume of 100 μl.

Quantification of gene expression in sorted ILC2 cells

Sorting for gene expression analysis by RT-qPCR was performed as described previously[50], with minor modifications. Briefly, ears and spleens from *Rag1*$^{-/-}$ mice were prepared and stained for flow cytometric analysis as described above. dILC2 were identified as DAPI$^-$CD45$^+$CD11b$^-$CD90^{hi}CD2$^-$ and splenic NK cells were sorted as DAPI$^-$CD11b^{lo}CD90$^+$NK1.1$^+$. $1–2 \times 10^3$ cells, depending on experiment, were sorted using a custom 10-laser Influx sorter (BD) into RLT plus lysis buffer (Qiagen). RNA was extracted using an RNeasy mini kit (Qiagen) and reverse-transcribed using Moloney murine leukemia virus-RT (Ambion) primed with random hexamers (GeneWorks, Australia). Quantitative PCR was performed using TaqMan Gene Expression Master Mix and the following Taqman assays: *Gapdh* (Mm99999915_g1), *Actb* (Mm00607939_s1), *Hprt* (Mm00446968_m1), *Il5* (Mm00439646_m1), *Il13* (Mm00434204_m1), *Gata3* (Mm00484683_m1). Target gene abundance was determined as a ratio of target gene expression normalized to the geometric mean of 3 reference genes (*Gapdh*, *Actb*, *Hprt*).

Histologic analysis of IL-2-treated skin

Ear pinnae and tail skin of untreated and IL-2-treated mice were fixed in 10% neutral buffered formalin. Following fixation in formalin, tissues were embedded in paraffin and 5-μm sections cut and stained with hematoxylin and eosin (H&E) or Toluidine Blue.

Statistical analysis

Data are presented as mean ± s.d. unless otherwise specified. Unpaired student's *t* test (normally distributed) was used to compare independent experimental groups unless otherwise specified. Statistics were computed with Prism5 (GraphPad Software). A difference was considered significant if $P < 0.05$.

Supplementary Material

Refer to Web version on PubMed Central for supplementary material.

Acknowledgments

References

1. Bieber T. Atopic dermatitis. N Engl J Med. 2008; 358:1483–1494. [PubMed: 18385500]

2. Li M, et al. Induction of thymic stromal lymphopoietin expression in keratinocytes is necessary for generating an atopic dermatitis upon application of the active vitamin D3 analogue MC903 on mouse skin. The Journal of investigative dermatology. 2009; 129:498–502. [PubMed: 18650845]

3. Spits H, et al. Innate lymphoid cells - a proposal for uniform nomenclature. Nature reviews Immunology. 2013; 13:145–149.

4. Chang YJ, et al. Innate lymphoid cells mediate influenza-induced airway hyper-reactivity independently of adaptive immunity. Nature immunology. 2011; 12:631–638. [PubMed: 21623379]

5. Mjosberg JM, et al. Human IL-25- and IL-33-responsive type 2 innate lymphoid cells are defined by expression of CRTH2 and CD161. Nature immunology. 2011; 12:1055–1062. [PubMed: 21909091]

6. Monticelli LA, et al. Innate lymphoid cells promote lung-tissue homeostasis after infection with influenza virus. Nature immunology. 2011; 12:1045–1054. [PubMed: 21946417]

7. Moro K, et al. Innate production of T(H)2 cytokines by adipose tissue-associated c-Kit(+)Sca-1(+) lymphoid cells. Nature. 2010; 463:540–544. [PubMed: 20023630]

8. Neill DR, et al. Nuocytes represent a new innate effector leukocyte that mediates type-2 immunity. Nature. 2010; 464:1367–1370. [PubMed: 20200518]

9. Price AE, et al. Systemically dispersed innate IL-13-expressing cells in type 2 immunity. Proceedings of the National Academy of Sciences of the United States of America. 2010; 107:11489–11494. [PubMed: 20534524]

10. Wong SH, et al. Transcription factor RORalpha is critical for nuocyte development. Nature immunology. 2012

11. Minty A, et al. Interleukin-13 is a new human lymphokine regulating inflammatory and immune responses. Nature. 1993; 362:248–250. [PubMed: 8096327]

12. Cohn L, et al. Th2-induced airway mucus production is dependent on IL-4Ralpha, but not on eosinophils. Journal of immunology. 1999; 162:6178–6183.

13. Grunig G, et al. Requirement for IL-13 independently of IL-4 in experimental asthma. Science. 1998; 282:2261–2263. [PubMed: 9856950]

14. Pope SM, et al. IL-13 induces eosinophil recruitment into the lung by an IL-5- and eotaxin-dependent mechanism. The Journal of allergy and clinical immunology. 2001; 108:594–601. [PubMed: 11590387]

15. Wilhelm C, et al. An IL-9 fate reporter demonstrates the induction of an innate IL-9 response in lung inflammation. Nature immunology. 2011; 12:1071–1077. [PubMed: 21983833]

16. Faulkner H, Humphreys N, Renauld JC, Van Snick J, Grencis R. Interleukin-9 is involved in host protective immunity to intestinal nematode infection. European journal of immunology. 1997; 27:2536–2540. [PubMed: 9368607]

17. Richard M, Grencis RK, Humphreys NE, Renauld JC, Van Snick J. Anti-IL-9 vaccination prevents worm expulsion and blood eosinophilia in Trichuris muris-infected mice. Proceedings of the National Academy of Sciences of the United States of America. 2000; 97:767–772. [PubMed: 10639154]

18. Shimbara A, et al. IL-9 and its receptor in allergic and nonallergic lung disease: increased expression in asthma. The Journal of allergy and clinical immunology. 2000; 105:108–115. [PubMed: 10629460]

19. Sumaria N, et al. Cutaneous immunosurveillance by self-renewing dermal gammadelta T cells. The Journal of experimental medicine. 2011; 208:505–518. [PubMed: 21339323]

20. Georgopoulos K, et al. The Ikaros gene is required for the development of all lymphoid lineages. Cell. 1994; 79:143–156. [PubMed: 7923373]

21. Kirstetter P, Thomas M, Dierich A, Kastner P, Chan S. Ikaros is critical for B cell differentiation and function. Eur J Immunol. 2002; 32:720–730. [PubMed: 11870616]

22. Muzumdar MD, Tasic B, Miyamichi K, Li L, Luo L. A global double-fluorescent Cre reporter mouse. Genesis. 2007; 45:593–605. [PubMed: 17868096]

23. Thomis DC, Gurniak CB, Tivol E, Sharpe AH, Berg LJ. Defects in B lymphocyte maturation and T lymphocyte activation in mice lacking Jak3. Science. 1995; 270:794–797. [PubMed: 7481767]

24. Barlow JL, et al. Innate IL-13-producing nuocytes arise during allergic lung inflammation and contribute to airways hyperreactivity. The Journal of allergy and clinical immunology. 2012; 129:191–198. e191–194. [PubMed: 22079492]

25. Hu-Li J, et al. Regulation of expression of IL-4 alleles: analysis using a chimeric GFP/IL-4 gene. Immunity. 2001; 14:1–11. [PubMed: 11163225]

26. Mjosberg J, et al. The transcription factor GATA3 is essential for the function of human type 2 innate lymphoid cells. Immunity. 2012; 37:649–659. [PubMed: 23063330]

27. Li M, et al. Topical vitamin D3 and low-calcemic analogs induce thymic stromal lymphopoietin in mouse keratinocytes and trigger an atopic dermatitis. Proceedings of the National Academy of Sciences of the United States of America. 2006; 103:11736–11741. [PubMed: 16880407]

28. Unutmaz D, et al. The primate lentiviral receptor Bonzo/STRL33 is coordinately regulated with CCR5 and its expression pattern is conserved between human and mouse. Journal of immunology. 2000; 165:3284–3292.

29. Possot C, et al. Notch signaling is necessary for adult, but not fetal, development of RORgammat(+) innate lymphoid cells. Nature immunology. 2011; 12:949–958. [PubMed: 21909092]

30. Ng LG, et al. Migratory dermal dendritic cells act as rapid sensors of protozoan parasites. PLoS Pathog. 2008; 4:e1000222. [PubMed: 19043558]

31. Hepworth MR, et al. Mast cells orchestrate type 2 immunity to helminths through regulation of tissue-derived cytokines. Proceedings of the National Academy of Sciences of the United States of America. 2012; 109:6644–6649. [PubMed: 22493240]

32. Livet J, et al. Transgenic strategies for combinatorial expression of fluorescent proteins in the nervous system. Nature. 2007; 450:56–62. [PubMed: 17972876]

33. Berrozpe G, et al. A distant upstream locus control region is critical for expression of the Kit receptor gene in mast cells. Mol Cell Biol. 2006; 26:5850–5860. [PubMed: 16847336]

34. Grimbaldeston MA, et al. Mast cell-deficient W-sash c-kit mutant Kit W-sh/W-sh mice as a model for investigating mast cell biology in vivo. Am J Pathol. 2005; 167:835–848. [PubMed: 16127161]

35. Biggs L, et al. Evidence that vitamin D(3) promotes mast cell-dependent reduction of chronic UVB-induced skin pathology in mice. The Journal of experimental medicine. 2010; 207:455–463. [PubMed: 20194632]

36. Halim TY, Krauss RH, Sun AC, Takei F. Lung natural helper cells are a critical source of Th2 cell-type cytokines in protease allergen-induced airway inflammation. Immunity. 2012; 36:451–463. [PubMed: 22425247]

37. Boyman O, Kovar M, Rubinstein MP, Surh CD, Sprent J. Selective stimulation of T cell subsets with antibody-cytokine immune complexes. Science. 2006; 311:1924–1927. [PubMed: 16484453]

38. Hoyler T, et al. The transcription factor GATA-3 controls cell fate and maintenance of type 2 innate lymphoid cells. Immunity. 2012; 37:634–648. [PubMed: 23063333]

39. Hamid Q, et al. In vivo expression of IL-12 and IL-13 in atopic dermatitis. The Journal of allergy and clinical immunology. 1996; 98:225–231. [PubMed: 8765838]

40. Zheng T, et al. Transgenic expression of interleukin-13 in the skin induces a pruritic dermatitis and skin remodeling. The Journal of investigative dermatology. 2009; 129:742–751. [PubMed: 18830273]

41. Ranson T, et al. IL-15 is an essential mediator of peripheral NK-cell homeostasis. Blood. 2003; 101:4887–4893. [PubMed: 12586624]

42. Malek TR. The biology of interleukin-2. Annual review of immunology. 2008; 26:453–479.

43. Wolf AI, et al. Plasmacytoid dendritic cells are dispensable during primary influenza virus infection. J Immunol. 2009; 182:871–879. [PubMed: 19124730]

44. von Freeden-Jeffry U, et al. Lymphopenia in interleukin (IL)-7 gene-deleted mice identifies IL-7 as a nonredundant cytokine. The Journal of experimental medicine. 1995; 181:1519–1526. [PubMed: 7699333]

45. Kennedy MK, et al. Reversible defects in natural killer and memory CD8 T cell lineages in interleukin 15-deficient mice. The Journal of experimental medicine. 2000; 191:771–780. [PubMed: 10704459]

46. Kleinschek MA, et al. IL-25 regulates Th17 function in autoimmune inflammation. The Journal of experimental medicine. 2007; 204:161–170. [PubMed: 17200411]

47. Herbst T, et al. Antibodies and IL-3 support helminth-induced basophil expansion. Proceedings of the National Academy of Sciences of the United States of America. 2012; 109:14954–14959. [PubMed: 22930820]

48. Al-Shami A, et al. A role for thymic stromal lymphopoietin in CD4(+) T cell development. The Journal of experimental medicine. 2004; 200:159–168. [PubMed: 15263024]

49. Roediger B, Ng LG, Smith AL, Fazekas de St Groth B, Weninger W. Visualizing dendritic cell migration within the skin. Histochem Cell Biol. 2008; 130:1131–1146. [PubMed: 18987873]

50. Mitchell AJ, et al. Technical advance: autofluorescence as a tool for myeloid cell analysis. J Leukoc Biol. 2010; 88:597–603. [PubMed: 20534703]
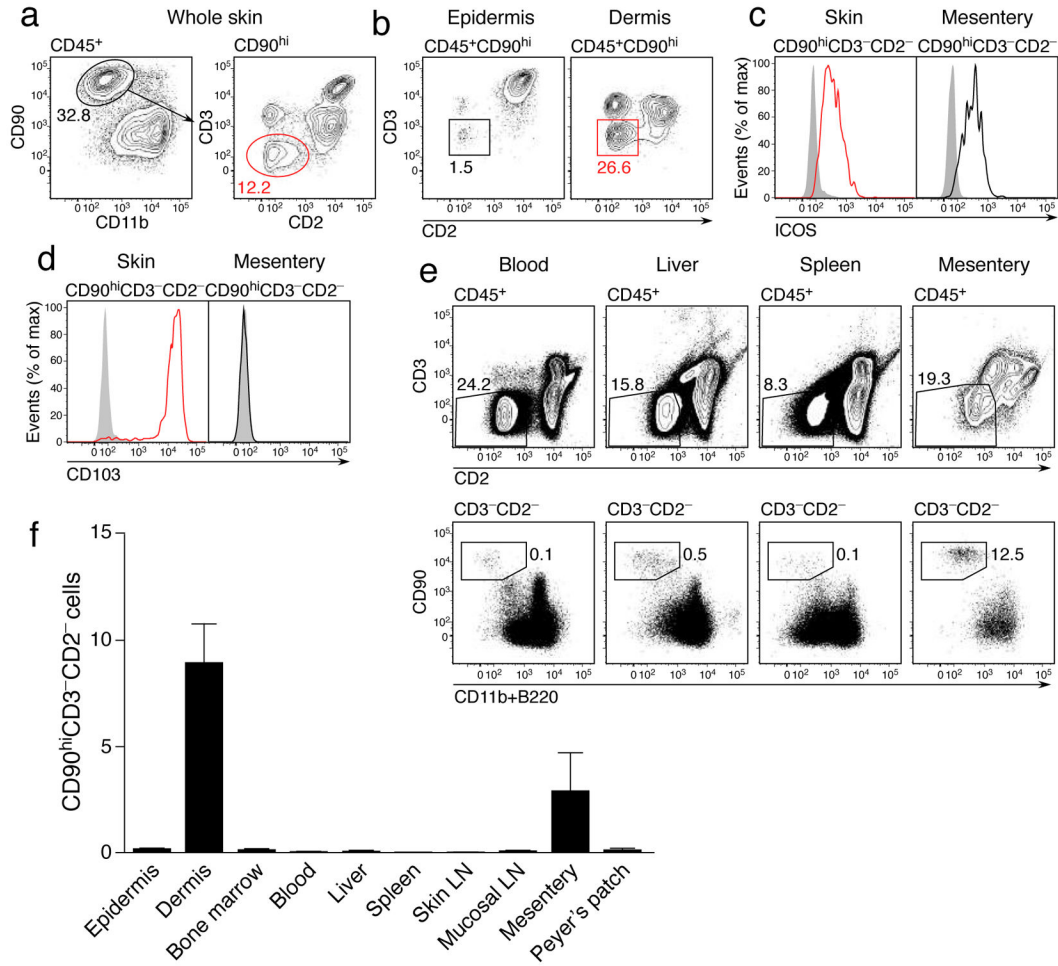
Figure 1. Identification and phenotype of dermal ILC2

(**a**) Representative contour plots of CD45^{+} CD11b^{lo} CD90^{hi} CD3^{−} CD2^{−} ILC2 within the skin of wild-type mice. Numbers indicate percent positive cells within each gate. Results representative of over 20 independent experiments. (**b**) Representative contour plots of ILC2 within the epidermis (left) and dermis (right) of wild-type mice. (**c**) Representative histograms depicting ICOS expression by ILC2 from the skin (left) and mesentery (right). (**d**) Representative histograms depicting CD103 expression by ILC2 from the skin (left) and mesentery (right). Results in (c) and (d) are representative of 2 independent experiments (n = 4). (**e**) Representative dotplots of CD45^{+} CD3^{−} CD2^{−} CD90^{hi} CD11b^{lo} B220^{−} ILC within the blood, liver, spleen and mesentery. (**f**) Relative abundance of ILC in indicated organs as a percentage of total isolated leukocytes. Data are mean ± s.d. and are pooled from 2 independent experiments (n = 3). LN, lymph node.
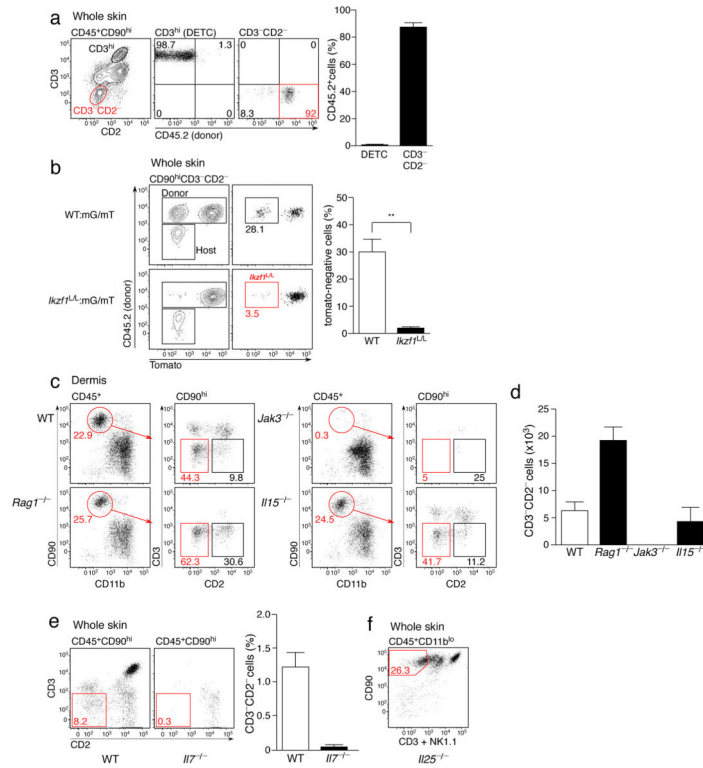
Figure 2. Development and homeostatic requirements of dILC2

(**a**) Representative dotplots (left) of mouse skin from CD45.1[+] mice 8 weeks post-irradiation and transfer of bone marrow from CD45.2[+] mice. Right: Percentages of DETC and dILC2 that were of donor-origin. Data are mean ± s.d. and are pooled from 2 independent experiments ($n = 7$). (**b**) Representative dotplots and graph depicting the relative contribution of donor (CD45.2^{+}) cells to dILC2 in 50:50 wild-type mG/mT(mTomato[+]):wild-type (CD45.2[+]) (top panels, open bar) and 50:50 wild-type mG/mT(mTomato[+]):*Ikzf1*[L/L] (CD45.2[+]) (bottom panels, filled bar) mixed bone marrow chimeras 8 weeks after bone marrow transfer into wild-type (CD45.1[+]) hosts. Data are mean ± s.d. and are representative of two independent experiments ($n = 3$ for control chimeras, $n = 2$ for wild-type:*Ikzf1*[L/L] chimeras). (**c**) Representative dotplots of CD45^{+} CD90^{hi} cells in the dermis of wild-type, *Rag1*^{−/−}, *Jak3*^{−/−} and *Il15*^{−/−} mice. Red boxes indicate CD3^{−}CD2^{−} dILC2. (**d**) Absolute numbers of dILC2 in the dermis of indicated mouse strains. Cell counts obtained from two ears. Data are mean ± s.d. and are representative of two independent experiments ($n = 3$). (**e**) Representative dotplots (left) and frequency (right) of dILC2 in wild-type and *Il7*^{−/−} skin. Data are mean ± s.d. ($n = 3$). (**f**) Representative dotplot of CD45^{+} CD11b^{lo} cells in the skin of *Il25*^{−/−} mice. Red gate indicates CD90^{hi} CD3^{−} NK1.1^{−} dILC2.
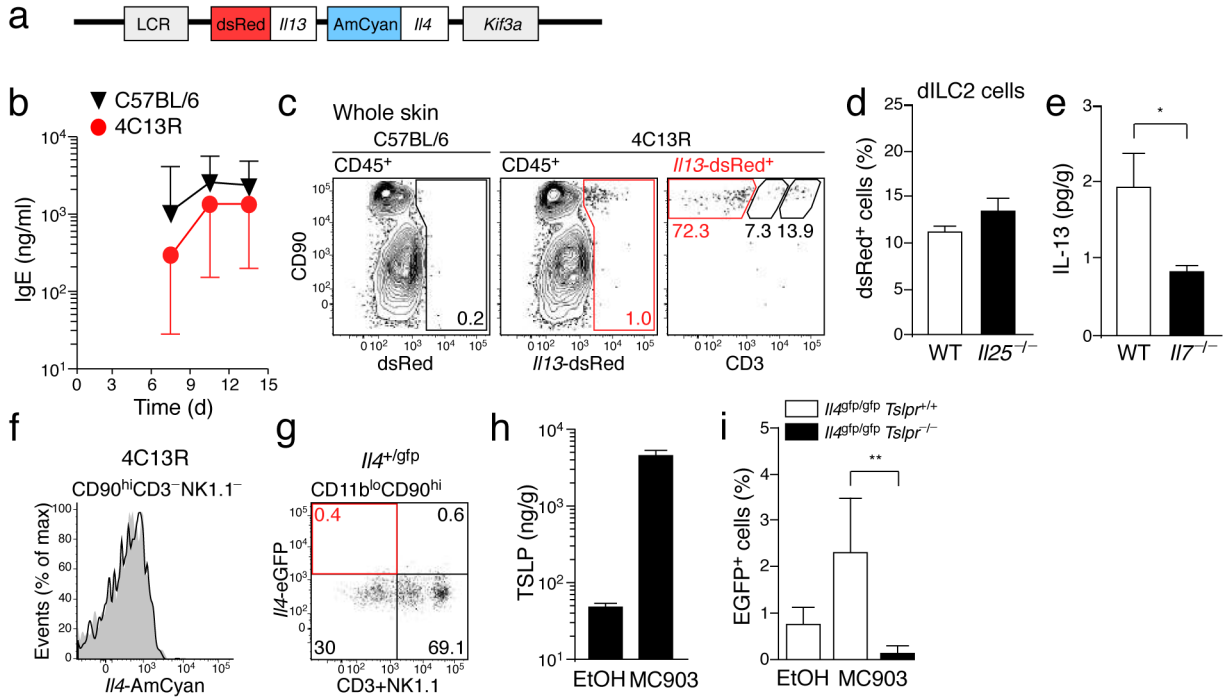
Figure 3. IL-13 production by dILC2 during the steady-state

(**a**) Schematic of the BAC-clone used to generate the dual reporter transgenic (4C13R) mice that express AmCyan under *Il4* regulatory elements and dsRed under *Il13* regulatory elements. LCR, Th2 locus control region; *Kif3a*, kinesin-related protein 3. (**b**) Serum IgE titers over the course of a *Nippostrongylus brasiliensis* infection in wild-type (black) and 4C13R transgenic (red) mice. IgE was not detected in uninfected mice (not shown). Data are geometric mean ± 95% CI ($n = 3$). (**c**) Representative dotplots of CD45$^+$ cells in the skin of wild-type (left) and 4C13R (middle) mice. Right: Phenotype of *Il13*-dsRed$^+$ cells in 4C13R skin. Red gate indicates CD90^{hi} CD3$^-$ NK1.1$^-$ dILC2. (**d**) Percentage of dILC2 that expressed *Il13*-dsRed in wild-type and *Il25*$^{-/-}$ 4C13R mice. (**e**) IL-13 protein in adult skin homogenates of wild-type (open bar) and *Il7*$^{-/-}$ (filled bar) mice, as detected by cytokine bead array. Data are mean ± s.d. ($n = 8$ for wild-type, $n = 6$ for *Il7*$^{-/-}$). *P = 0.0337 (one-tailed unpaired *t*-test). (**f**) Representative histogram of *Il4*-AmCyan expression by dILC2 in 4C13R mice (black line) compared to non-transgenic control (grey histogram). Data are representative of over 10 independent experiments. (**g**) Representative dotplot depicting eGFP expression by CD45$^+$ CD11b^{lo} CD90^{hi} cells in the skin of *Il4*$^{+/gfp}$ knockin mice. Gates were set using a non-transgenic control. Data are representative of 2 independent experiments. (**h**) TLSP protein in skin homogenates of MC903-treated mice and vehicle (ethanol, EtOH) treated controls, as detected by ELISA. Data are mean ± s.d. ($n = 5$ for MC903, $n = 4$ for EtOH). (**i**) Percentage of *Il4*-eGFP$^+$ dILC2 in *Il4*$^{gfp/gfp}$ (open bars) and *Il4*$^{gfp/gfp}$ *Tslpr*$^{-/-}$ (filled bar) mice topically treated with MC903. Data are mean ± s.d. (*Il4*$^{gfp/gfp}$ EtOH and MC903, $n = 4$; *Il4*$^{gfp/gfp}$ *Tslpr*$^{-/-}$ MC903, $n = 5$). **P = 0.0047 (unpaired *t* test).
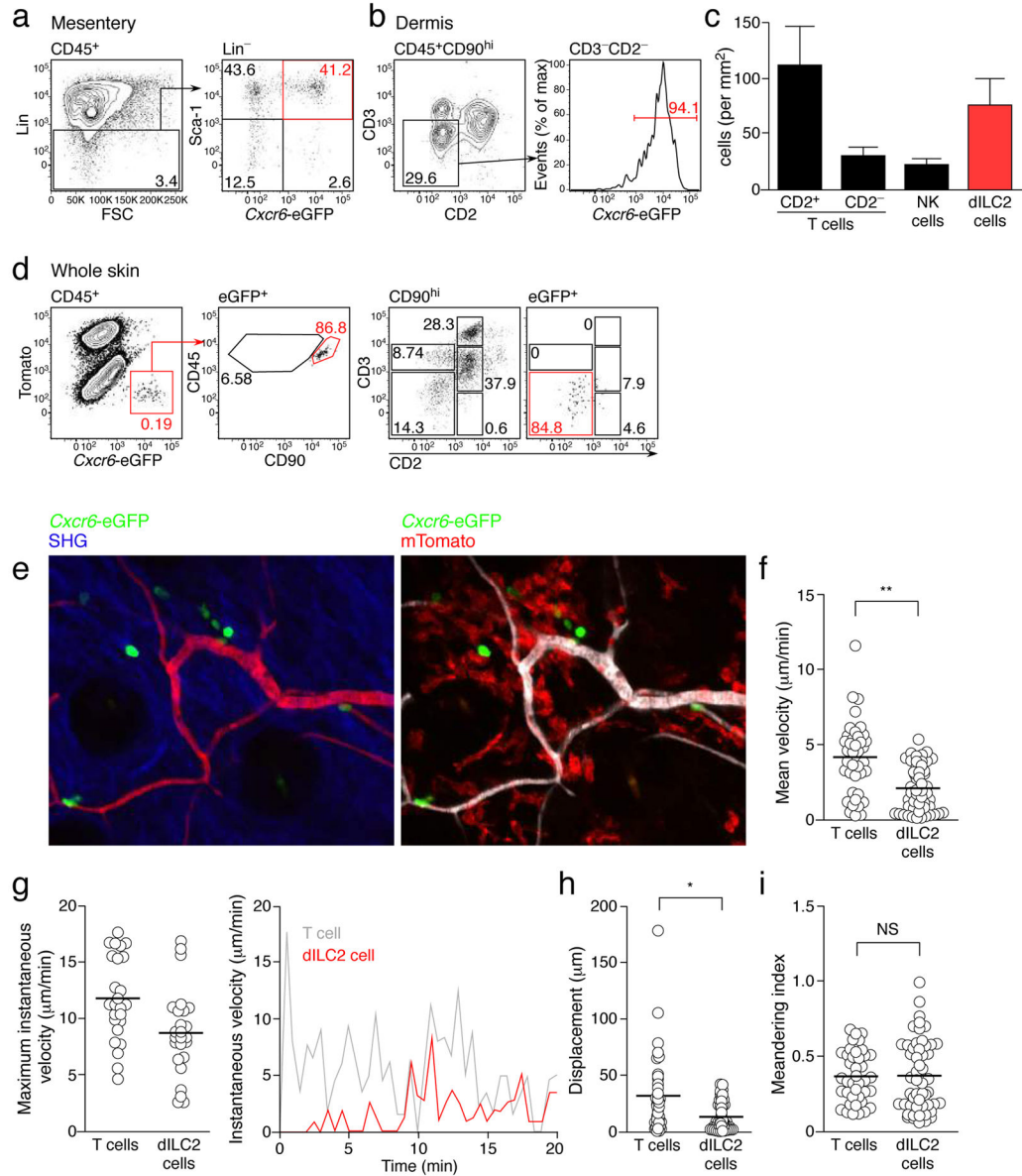
Figure 4. Visualization of dILC2 *in vivo*

(**a**) Representative dotplots depicting the identification of Lin− Sca-1+ natural helper cells[7] from the mesentery of *Cxcr6*+/gfp mice. (**b**) Left: Representative contour plots of CD45+ CD90hi cells in the skin of *Cxcr6*+/gfp mice. Gate indicates CD2− CD3− dILC2. Right: Histogram showing eGFP expression by dILC2. Data are representative of over 10 independent experiments. (**c**) Density of indicated cell subsets within the ear of *Cxcr6*+/gfp mice. Counting was performed using multiphoton microscopy and flow cytometry (see Supplementary Methods). Data are mean ± s.d. and are representative of 2 independent experiments. (**d**) Representative dotplots of CD45+ (left) and eGFP+ cells (second left and far right panels) from the skin of albino C57BL/6 mice 8 weeks after irradiation and co-transfer of bone marrow from *Rag1*−/− *Cxcr6*+/gfp and RAG-1-sufficient mG/ mT(mTomato+) mice. Gates applied to eGFP+ cells were determined on total CD45+

population. (**e**) Representative images of mixed chimeric mouse skin by intravital multiphoton microscopy. Each image is a *z*-projection through a volume of 28 μm within the dermis. Extracellular matrix in the dermis was detected by second harmonic generation (SHG) signals (blue). Blood vessels were visualized using Evans blue. dILC2 shown in green. (**f**) Mean velocity of T cells and dILC2. (**g**) Left: Maximum instantaneous velocity of T cells and dILC2 measured during the imaging period. Right: Representative graph of instantaneous velocity of a single T cell (grey line) and a single ILC2 (red line) over 20 min. (**h**) Displacement of T cells and dILC2 over 15 minutes. (**i**) Meandering index of T cells and dILC2. Data in (f), (g), (h) and (i) are pooled from 4 independent experiments (T cells, *n* = 39; dILC2, *n* = 51). Symbols represent individual cells. *P < 0.001 and **P < 0.0001 (unpaired *t*-test). NS, not significant.
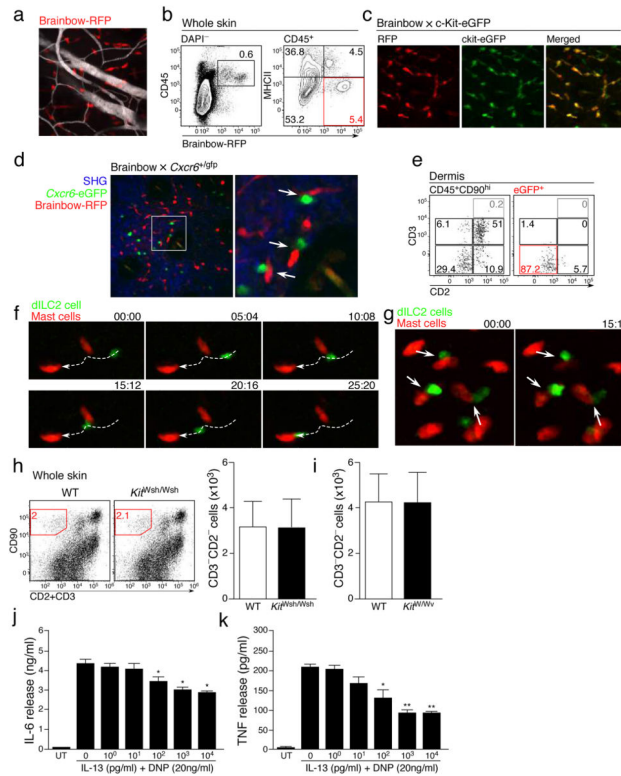
Figure 5. dILC2 interaction with skin-resident mast cells

(**a**) Representative image of the Brainbow[32] dermis by intravital multiphoton microscopy. Blood vessels were visualized using Evans blue (white). Image is a *z*-projection through a dermal volume of 60μm. (**b**) Representative flow cytometry plots of total skin cells (left) and CD45^{+} cells (right) from a Brainbow mouse. Red gate indicates RFP^{hi} MHC-II^{lo} cells. Data are representative of 3 independent experiments. (**c**) Representative images of the dermis from Brainbow × c-Kit-eGFP[33] mice. RFP^{+} cells, red. eGFP^{+} mast cells, green. Double-positive cells, yellow. (**d**) Representative image of Brainbow × *Cxcr6*[+/gfp] skin by intravital multiphoton microscopy. Extracellular matrix in the dermis was detected by SHG signals (blue). *Cxcr6*-eGFP^{+} cells shown in green. RFP^{+} cells are red. Arrows indicate RFP^{hi} mast cells in close proximity with eGFP^{+} cells. (**e**) Representative dotplots of CD45^{+}CD90^{hi} (left) and eGFP^{+} cells (right) from the skin of an albino Brainbow mice 8 weeks after irradiation and co-transfer of bone marrow from *Rag1*^{−/−} *Cxcr6*[+/gfp] and RAG-1-sufficient non-fluorescent mice. Gates for eGFP^{+} cells in right panel were determined on the total CD45^{+}CD90^{hi} population (left). (**f**) Representative time-lapse images of migratory dILC2 (green) in chimeric mouse skin by intravital multiphoton microscopy. Red, mast cells. White line, track of ILC2 migration during the observation period. Time shown in mm:ss. (**g**) Representative time-lapse images of chimeric mouse skin by intravital multiphoton microscopy. Arrows indicate dILC2 (green) that formed extended interactions with mast cells (red) throughout the observation period. Time shown in mm:ss. (**h**) Representative dotplots (left) and absolute number (right) of CD90^{hi} CD3^{−} CD2^{−} dILC2 in wild-type and B6-*Kit*[W-sh/W-sh] ears. (**i**) Absolute number dILC2 in wild-type and WBB6F$_1$-*Kit*[W/W-v] ears. Data in (i) and (j) are mean ± s.d. (*n* = 3). (**j** and **k**) Effect of exogenous IL-13 on cytokine

production by mast cells *in vitro*. Mast cells were pre-incubated with mrIL-13 (0–10,000 pg/ml), sensitized with anti-DNP IgE (2 µg/ml) for 16 h, washed then stimulated with DNP-HSA (20 ng/ml) in the presence of rmIL-13 (0 – 10000 pg/ml) for 6 h. (**j**) IL-6 and (**k**) TNF in supernatant were measured by ELISA. Data in (k) and (l) are expressed as mean ± s.e.m. for 3 independent experiments. Significant differences between cytokine release by DNP alone and in the presence of IL-13 were determined by one way ANOVA with Dunnett's post-test. * P < 0.01, **P < 0.001.
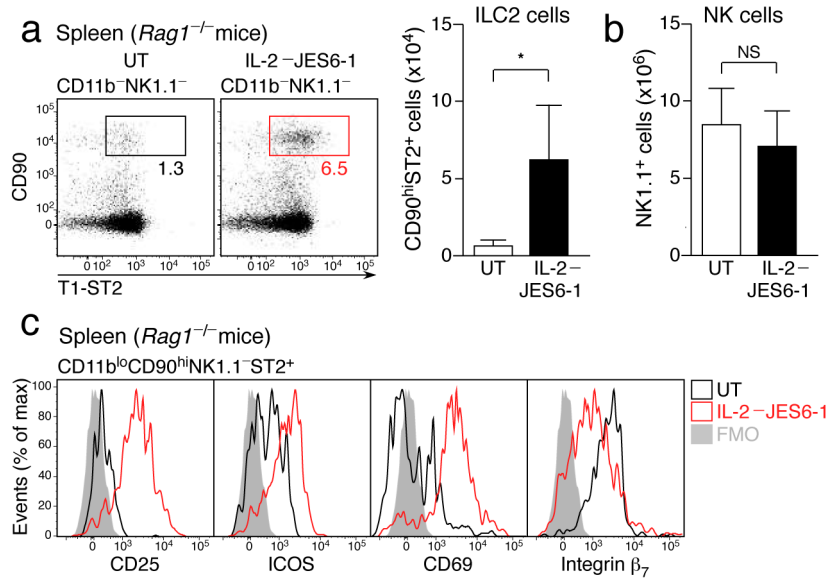
Figure 6. IL-2 induced activation and proliferation of ILC2 *in vivo*.
(**a**) Left: Representative dotplots of CD11b^{−} NK1.1^{−} splenocytes from IL-2–JES6-1 treated *Rag1*^{−/−} mice and untreated controls. Boxes indicate percentage of CD90^{hi} ST2^{+} ILC2. Right: Absolute number of splenic ILC2 from IL-2–JES6-1 treated mice compared to untreated controls. (**b**) Absolute number of splenic NK1.1^{+} NK cells in IL-2–JES6-1 treated *Rag1*^{−/−} mice and untreated controls. (**c**) Representative histograms depicting surface marker expression by splenic ILC2 from untreated (black) and IL-2–JES6-1 treated (red) *Rag1*^{−/−} mice. FMO, "fluorescence minus one" control. Data in (a) and (b) are mean ± s.d. and are representative of three independent experiments (untreated, *n* = 4; IL-2–JES6-1, *n* = 5). *P = 0.0180 (unpaired *t*-test). NS, not significant.
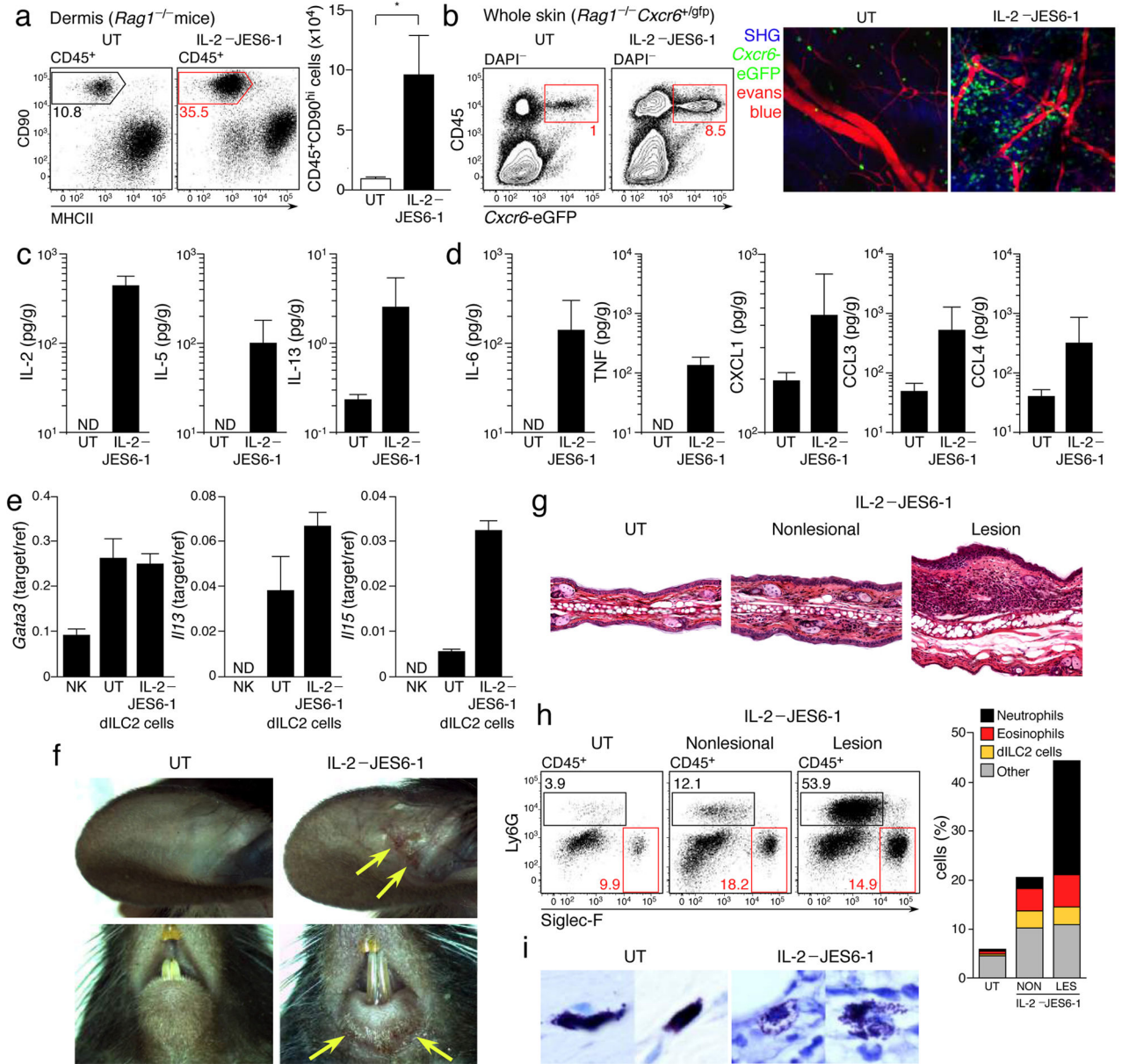
Figure 7. IL-2 stimulation of dILC2 *in vivo*.
(**a**) Left: Representative dotplots of dermal leukocytes isolated from IL-2–/JES6-1 treated *Rag1*^{−/−} mouse ears and untreated controls. Gates indicate percentage of CD90^{hi} dILC2. Right: Absolute number of CD45^{+}CD90^{hi} dILC2 from IL-2–JES6-1 treated mice compared to untreated controls. Data are mean ± s.d. and are representative of two independent experiments (untreated, *n* = 4; IL-2/JES6-1, *n* = 5). *P = 0.0015 (unpaired *t*-test). (**b**) Left: Representative dotplots of skin cells isolated from IL-2–JES6-1 treated *Rag1*^{−/−} *Cxcr6*[+/gfp] mice and untreated controls. Gates indicate percentage of eGFP[+] dILC2. Right: Representative images of IL-2–JES6-1 treated and untreated *Rag1*^{−/−} *Cxcr6*[+/gfp] mouse skin by intravital multiphoton microscopy. Each image is a *z*-projection through a volume of 88 μm within the dermis. Extracellular matrix in the dermis was detected by SHG signals

(blue). Blood vessels were visualized using Evans blue (red). dILC2 shown in green. (**c** and **d**) Cytokine concentrations in adult tail skin homogenates of IL-2–JES6-1 treated $Rag1^{-/-}$ mice and untreated controls, as detected by cytokine bead array. Data are geometric mean ± 95% CI and are pooled from three independent experiments (untreated, n = 9; IL-2/JES6-1, n = 12). (**e**) *Gata3*, *Il13* and *Il5* mRNA expression by sorted dILC2 from untreated and IL-2–JES6-1 treated $Rag1^{-/-}$ mice, as measured by real-time PCR. Splenic NK cells were included for comparison. (**f**) Representative macroscopic images of spontaneous skin lesions (yellow arrows) observed in mice treated with IL-2–JES6-1. (**g**) Ear sections obtained from untreated and IL-2-treated $Rag1^{-/-}$ mice, stained with hematoxylin and eosin. (**h**) Left: Representative flow cytometry dotplots of leukocytes isolated from lesional and non-lesional skin of IL-2-treated $Rag1^{-/-}$ mice. Boxes indicate Ly6G$^+$ neutrophils (black) and Siglec-F$^+$ eosinophils (red). Right: Proportion of neutrophils, eosinophils and dILC2 in lesional and non-lesional skin of IL-2-treated $Rag1^{-/-}$ mice compared to an untreated control. (**i**) Representative tail sections obtained from untreated and IL-2-treated $Rag1^{-/-}$ mice, stained with toluidine blue.

Table 1

Cell surface profile of *in vivo*-activated ILC2

Summary of cell surface expression (flow cytometry) of indicated proteins by ILC2 from untreated and IL-2–JES6-1 treated mice. −, not detected; +, positive; hi, high expression; lo, low expression. Data summarized from 2 independent experiments ($n = 4$).

	UT	IL-2–JES6-1
CD25	+	hi
ICOS	+	hi
T1-ST2	lo	hi
CD69	lo	hi
Integrinβ$_7$	hi	lo
CD49d	lo	−
CD49e	lo	lo
KLRG1	hi	hi
NKG2D	−	−
NKp46	−	−
CD84	+	+
CD103	−	−
IL13Rα1	+	+
FcεR1	−	−